Laminate Design for Coupled Wind Turbine Blades

James E. Locke*and Thomas M. Hermann†

National Institute for Aviation Research,
Wichita State University, Wichita, Kansas, 67260-0093

The purpose of this paper is to demonstrate the effect of coupling at the laminate level on coupling at the structural level. Four extension-shear coupled laminates are examined. The laminates are then used in structures with circular, square and airfoil cross-sections. The properties of those cross-sections are used to describe a general elastic beam using a method from Kosmatka. The coupling properties of the beam are compared with those of the laminate using a normalized coupling coefficient, stiffness coupling ratio and compliance coupling ratio. The normalized compliance ratio compared well between the laminate and the cross-sections for all cases.

Nomenclature

α	Coupling coefficient.
$\delta\Pi$	Virtual work.
ϵ	Axial strain.
γ	Shear strain.
κ	"beam" strain.
σ	Axial stress.
τ	Shear stress.
A	Laminate extensional stiffness matrix.
C	Material constitutive matrix.
D	Cross-sectional stiffness matrix.
E	Axial modulus.
G	Shear modulus.
N	Shape function.
S	Laminate compliance matrix.
S_{16}/S_{11}	Shear coupling ratio.
u	x displacement.
$U(x,y)$	x warping function.
v	y displacement.
$V(x,y)$	y warping function.
w	z displacement.
$W(x,y)$	z warping function.
C	Carbon.
CLT	Classical lamination theory.
DB	Double bias.

I. Introduction

Modern wind turbines are being designed with blades approaching 100-m and greater in length. The mass of blades is proportional to the length by as little as a power of 2.3[1] and as much as 3.[2] In either case, it is desirable to minimize the weight of the blade, and thereby the cost. As noted in Reference,[1] methods for minimizing the weight include employing alternative composite materials such as carbon fiber[3,4] and introducing twist-bend coupling to passively alleviate loads on the blades.[5–11] Effective design of twist-bend coupled blades requires understanding the correspondence between laminate schedule design, cross section coupling and thereby global blade behavior.

A correspondence between the laminate shear coupling ratio, S_{16}/S_{11}, and the blade section coupling will be presented in this paper. The shear coupling ratio will be directly calculated from the constitutive

*Director, Research and Development; Airbus Engineering Faculty Fellow; Associate Fellow AIAA; James.Locke@wichita.edu
†Research Associate; Member AIAA; Thomas.Hermann@wichita.edu

laminate properties using classical lamination theory(CLT). The cross-sectional coupling properties will be calculated using a procedure developed by Kosmatka[12] for arbitrary cross-sections with extension-bending-torsion coupling

Four coupled, hybrid, laminate types are examined, listed in Table 1. The laminates are constructed from 6 layers of $15oz/yd^2$ unidirectional carbon between two layers of $12oz/yd^2$ double bias glass fabric. Four of the layers are rotated to introduce coupling. Four angles were examined, 10, 15, 20 and 25 degrees. Tension, compression and shear tests of these laminates have been performed at the National Institute for Aviation Research (NIAR) to determine the elastic moduli.

II. Laminate Coupling

For blade designs with bend-twist coupling the level of coupling at the laminate level can be quantified using either the laminate compliance matrix, $[S]$, or the laminate extensional stiffness matrix, $[A]$.[13] The resulting extensional strains can be written in terms of the "average laminate stresses" as

$$\begin{Bmatrix} \epsilon_{xx} \\ \epsilon_{yy} \\ \gamma_{xy} \end{Bmatrix} = \begin{bmatrix} S_{11} & S_{12} & S_{16} \\ S_{12} & S_{22} & S_{26} \\ S_{16} & S_{26} & S_{66} \end{bmatrix} \begin{Bmatrix} \bar{\sigma}_{xx} \\ \bar{\sigma}_{yy} \\ \bar{\tau}_{xy} \end{Bmatrix} \tag{1}$$

The extensional and shear strains corresponding to an axial stress state ($\bar{\sigma}_{xx} \neq 0$, $\bar{\sigma}_{yy} = \bar{\tau}_{xy} = 0$) can be written as

$$\begin{aligned} \epsilon_{xx} &= S_{11}\bar{\sigma}_{xx} \\ \gamma_{xy} &= S_{16}\bar{\sigma}_{xx} \end{aligned} \tag{2}$$

This results in a shear strain to axial strain ratio of

$$\gamma_{xy}/\epsilon_{xx} = S_{16}/S_{11} \tag{3}$$

where S_{16}/S_{11} is the laminate shear coupling ratio, which represents the shear strain per unit axial strain.

The laminate shear coupling ratio is listed in Table 2 and plotted in Figure 1. Reviewing Table 1, laminate 1 is the uncoupled basis laminate against which to compare laminates 2 through 5 which have varying amounts of off-axis layers. Four layers are oriented off-axis 10° in laminate 2, 15° in laminate 3, 20° in laminate 4 and 25° in laminate 5. With increasing angle, there is an acceleration in reduction of the axial stiffness. The shear coupling ratio is maximum at 15° in laminate 3 and decreases after that. Laminate 2, with 0.86 of the axial stiffness of laminate 1, exhibits a shear coupling ratio approximately equal to laminate 4, which has 0.61 of axial stiffness of laminate 1.

III. Section Coupling

The current cross-sectional modeling procedure is based on the approach presented by Kosmatka[12] for arbitrary cross-sections with extension-bending-torsion coupling. Cross-sectional properties are determined in terms of four strain measures: extension, two bending curvatures, and twisting. These four stain measures are used in conjunction with generalized warping functions that are determined by applying the principle of virtual work.

III.A. Cross-Sectional Stiffness Matrix

The beam cross-section, Figure 2, is assumed to lie in the x-y plane with axial loading P in the z direction, bending moments M_x and M_y about the x and y axes, and torsion T about the z axis. For these stress resultants the beam x-y-z displacements (u, v, w) are assumed to be of the form:

$$\begin{aligned} u(x,y,z) &= -yz\theta + \frac{z^2}{2}\kappa_x + U(x,y) \\ v(x,y,z) &= xz\theta - \frac{z^2}{2}\kappa_y + V(x,y) \\ w(x,y,z) &= ze - xz\kappa_x + yz\kappa_y + W(x,y) \end{aligned} \tag{4}$$

Table 1. Composite laminates.

Laminate	Schedule	Angle	Behavior
1	$[\pm 45_{DB}/(0_C)_3]_s$	0	Quasi-Orthotropic
2	$[\pm 45_{DB}/(10_C)_2/0_C]_s$	10	Coupled, Extension/Shear
3	$[\pm 45_{DB}/(15_C)_2/0_C]_s$	15	Coupled, Extension/Shear
4	$[\pm 45_{DB}/(20_C)_2/0_C]_s$	20	Coupled, Extension/Shear
5	$[\pm 45_{DB}/(25_C)_2/0_C]_s$	25	Coupled, Extension/Shear

Table 2. Effect of coupling on axial modulus.

Laminate	E_x (GPA)	E_y (GPa)	G_{xy} (GPa)	E_x Reduction	$\frac{S_{16}}{S_{11}}$
1	106.4	10.26	6.00	1.00	0.000
2	87.9	10.27	6.72	0.83	-1.300
3	74.9	10.34	7.60	0.70	-1.417
4	64.7	10.50	8.75	0.61	-1.327
5	57.3	10.80	9.98	0.54	-1.150

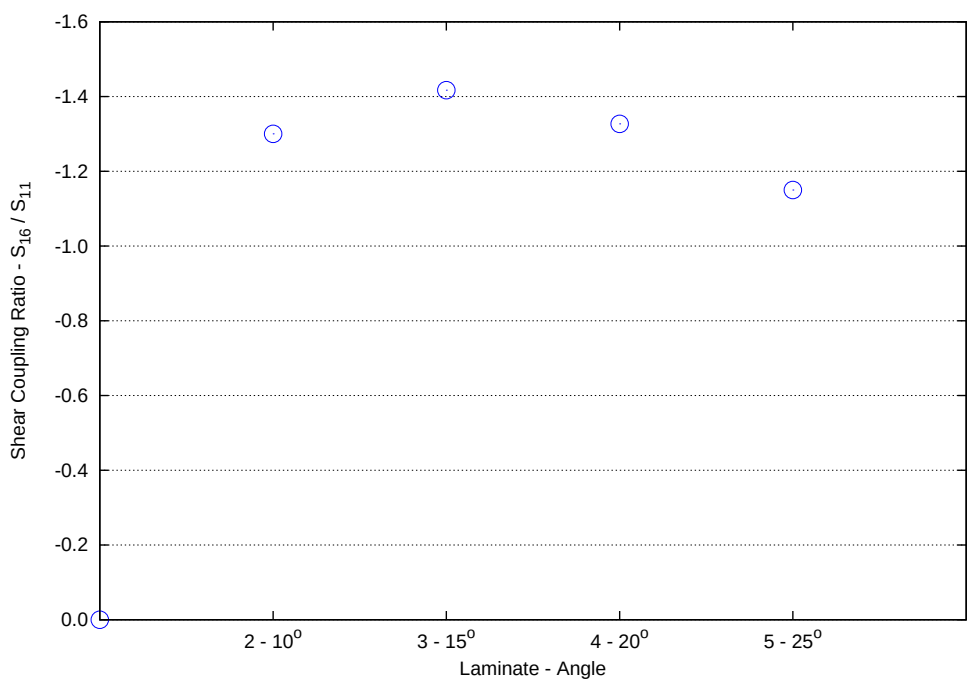

Figure 1. Effect of the angle of the off-axis plies on the level of coupling.

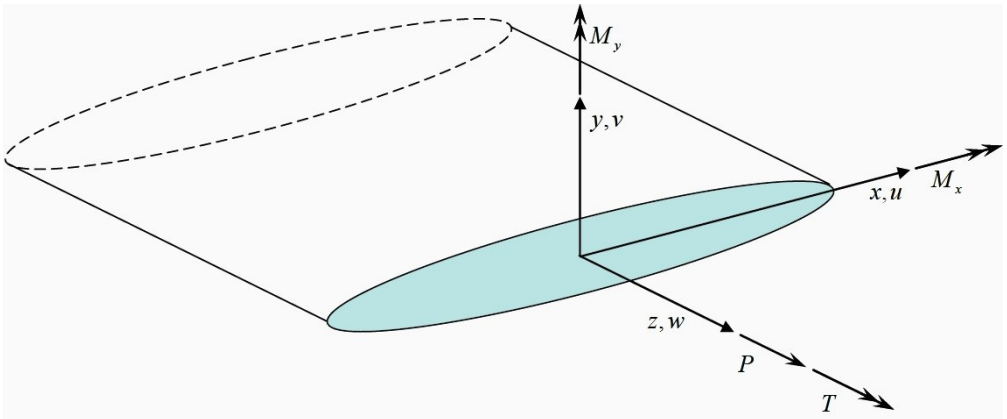

Figure 2. Beam cross-section coordinate system, stress resultants, and displacements.

where e, κ_x, κ_y and θ are the "beam" strain measures and the two-dimensional warping functions U, V, and W are added to accommodate both in-plane and out-of-plane changes in shape that are compatible with the beam strain measures. Expressions for U, V, and W can be determined using the finite element method. The basic approach consists of the following steps:

1. Create a two-dimensional finite element model of the beam cross-section.
2. Determine the displacements U, V, and W corresponding to unit strain measures.
3. Integrate the stresses over the cross-section to determine the cross-sectional stiffness matrix $[D]$, where $\{F\} = [D]\{h\}$

with

$$\{F\}^T = \{P \quad M_y \quad M_x \quad T\}$$
$$\{h\}^T = \{e \quad \kappa_x \quad \kappa_y \quad \theta\}$$

For completeness, a description of the detailed finite element procedure is given in Appendix A.

III.B. Cross-Sectional Modeling

Five different cross-sections, Figure 3, were modeled in order to evaluate the difference between laminate coupling and cross-sectional coupling. Laminate 1 is the uncoupled laminate from Table 1; laminates 2 through 5, also listed in Table 1, have varying amounts of coupling. Finite element meshes for these cross-sections are shown in Figure 4. Note that the thickness is not to scale. All of the meshes were generated using three grid(or node) points through the thickness of the laminate, which resulted in approximately 600 grids with 3 degrees-of-freedom at each grid.

III.C. Cross-Sectional Coupling

As previously mentioned laminate level coupling can be examined based on the laminate shear coupling ratio S_{16}/S_{11}. The results shown in Figure 1 indicate a maximum level of coupling for laminate 3 which has an angle of 15°. The cross-sectional coupling can be determined based on the cross-sectional stiffness matrix, $[D]$. Bend-twist coupling between the bending moment M_x and the torsion T is due to the stiffness term D_{34}. Coupling results for wind blade applications have typically been presented in terms of the coupling coefficient α, which is defined as[5]

$$\alpha = -D_{34}/\sqrt{D_{33}D_{44}} \tag{5}$$

For the cross-sections shown in Figure 3, coupling coefficients for the 4 laminate styles are given in Table 3. Normalized values were also calculated by dividing the actual α value by the maximum α value, $\alpha_{\max}$, for the given cross-section. These normalized coupling coefficients are plotted in Figure 5.

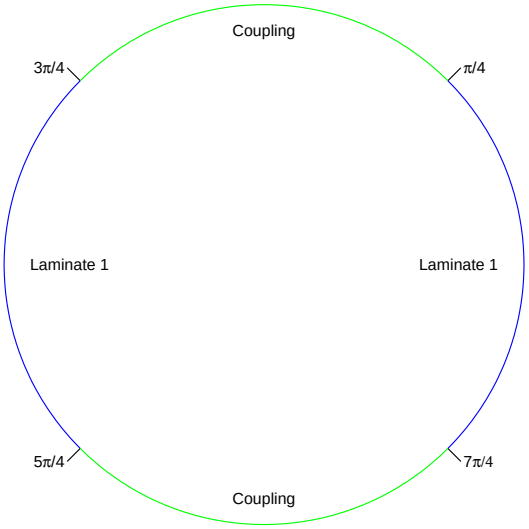

(a) Circle

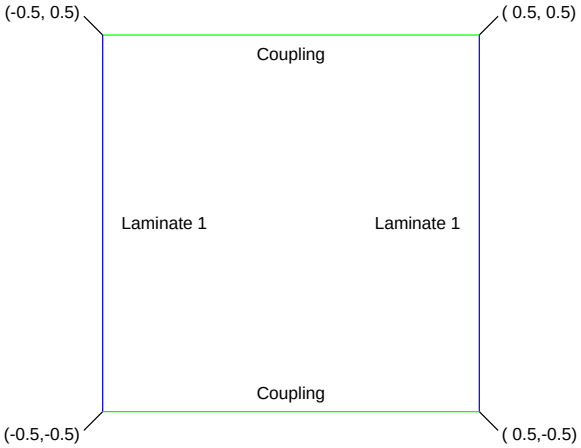

(b) Square

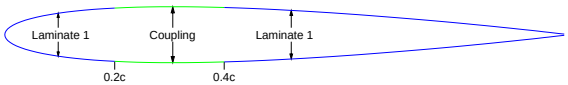

(c) Single-Cell

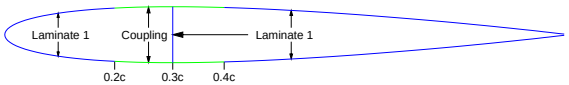

(d) Two-Cell

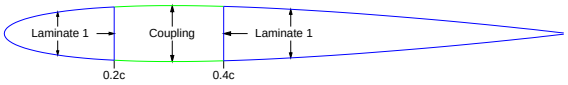

(e) Three-Cell

Figure 3. Coupled cross-sections.

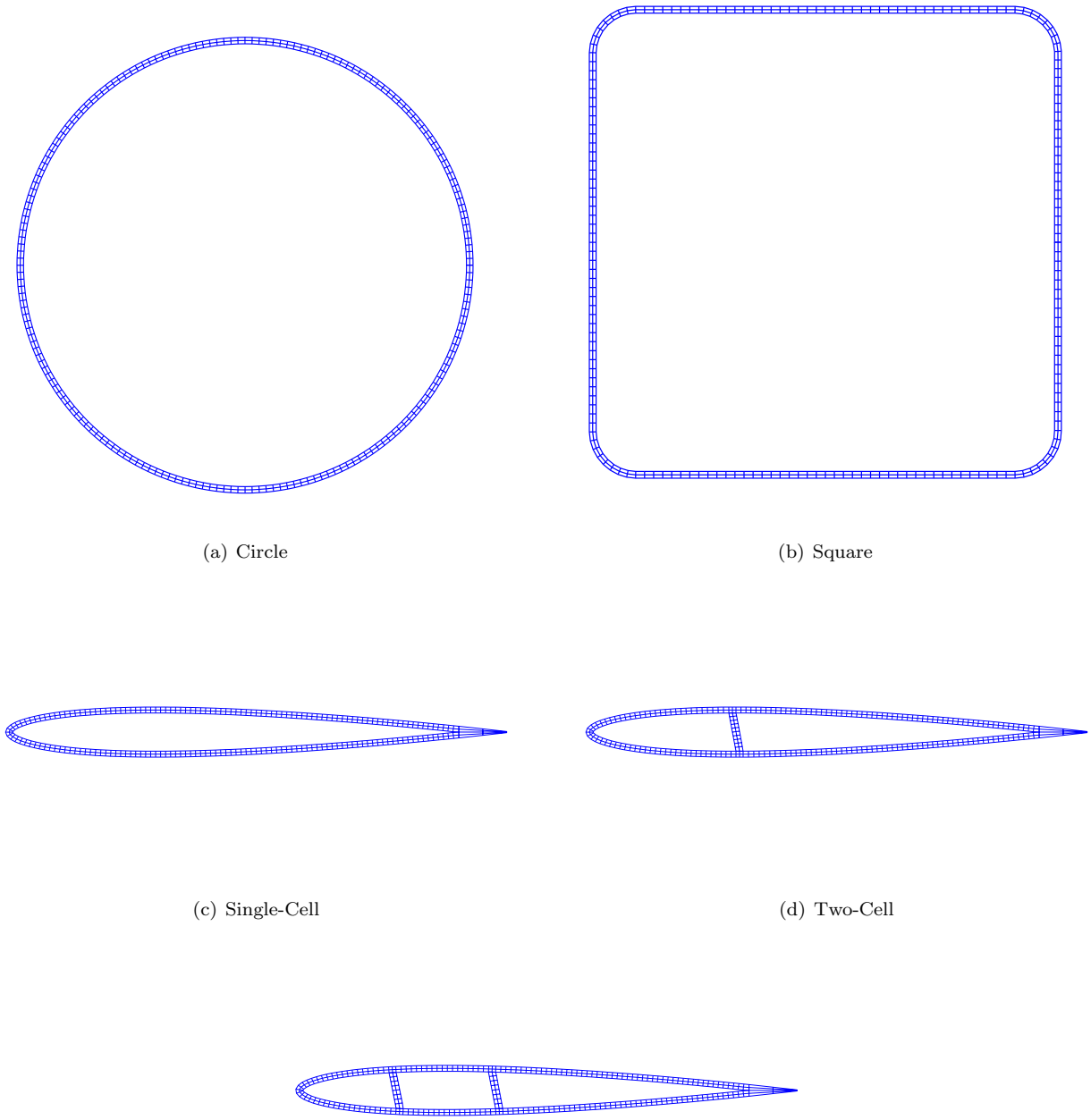

(a) Circle

(b) Square

(c) Single-Cell

(d) Two-Cell

(e) Three-Cell

Figure 4. Cross-section meshes.

Table 3. Cross-sectional coupling coefficient.

				NACA 0012		
Laminate	Angle	Box	Circular	Single-Cell	Two-Cell	Three-Cell
Coupling coefficient α						
2	10	0.213	0.220	0.087	0.088	0.116
3	15	0.254	0.263	0.098	0.100	0.141
4	20	0.258	0.269	0.095	0.097	0.144
5	25	0.238	0.249	0.084	0.086	0.133
Normalized coupling coefficient $\alpha/\alpha_{\max}$						
2	10	0.824	0.817	0.883	0.879	0.804
3	15	0.984	0.980	1.000	1.000	0.977
4	20	1.000	1.000	0.966	0.969	1.000
5	25	0.924	0.928	0.856	0.860	0.921

Laminate coupling coefficients were computed using three approaches. The first approach uses the laminate coupling ratio, S_{16}/S_{11}, from Figure 1. The second approach is based on a laminate level coupling coefficient that is calculated from the laminate extensional stiffness matrix, $[A]$. This coefficient, denoted as α_1, is defined as

$$\alpha_1 = A_{16}/\sqrt{A_{11}A_{66}} \tag{6}$$

The third approach is based on a laminate level coupling coefficient that is calculated from the reduced laminate extensional stiffness matrix, $[A^*]$. This coefficient, denoted as α_2, is defined as

$$\alpha_2 = A^*_{16}/\sqrt{A^*_{11}A^*_{66}} \tag{7}$$

where

$$\begin{bmatrix} A^*_{11} & A^*_{16} \\ A^*_{16} & A^*_{66} \end{bmatrix} = \begin{bmatrix} S_{11} & S_{16} \\ S_{16} & S_{66} \end{bmatrix}^{-1}$$

This approach is based on the assumption that the laminate average stress in the y-direction is equal to zero ($\bar{\sigma}_{yy} = 0$). These three laminate coupling coefficients are listed in Table 4 and plotted in Figure 5. The cross-sectional and laminate coupling results shown in Figure 5 indicate that the laminate coupling coefficients, equations 3, 6 and 7, do not correlate well with the cross-sectional coupling coefficient, equation 5.

Table 4. Laminate coupling coefficient.

Laminate	Angle	S_{16}/S_{11}	α_1	α_2
Actual value				
2	10	1.300	0.367	0.359
3	15	1.417	0.470	0.452
4	20	1.327	0.527	0.488
5	25	1.150	0.552	0.480
Normalized value				
2	10	0.917	0.664	0.737
3	15	1.000	0.852	0.925
4	20	0.936	0.956	1.000
5	25	0.812	1.000	0.983

Two more alternatives for comparing cross-sectional and laminate coupling results are: (1) a comparison of the stiffness ratios, and (2) a comparison of the compliance ratios. The cross-sectional stiffness ratio is defined as D_{34}/D_{33}. Cross-sectional stiffness ratios for the 4 laminate styles are given in Table 5 and plotted

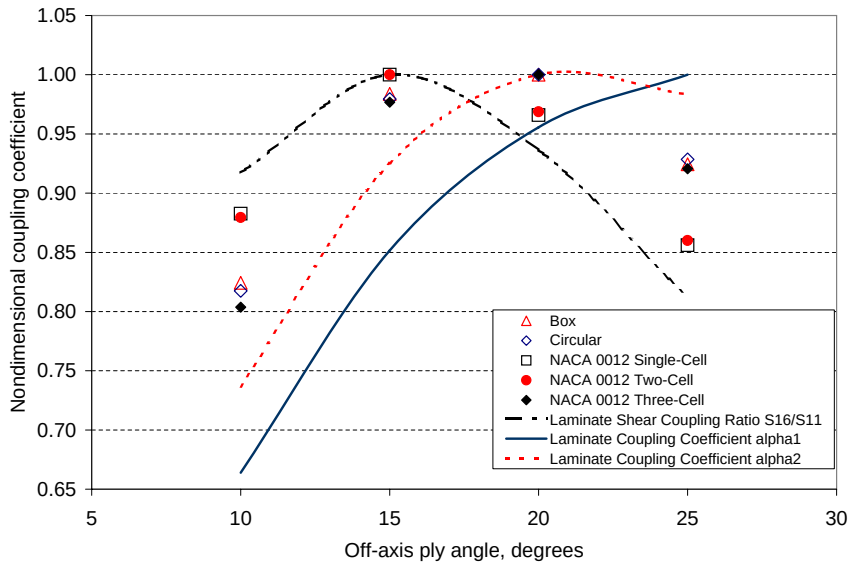

Figure 5. Comparison of cross-sectional coupling coefficient with laminate coupling coefficient.

in Figure 6. For the laminate the two stiffness ratios are defined as A_{16}/A_{11} and A^*_{16}/A^*_{11}. Values for these stiffness ratios are given in Table 6 and plotted in Figure 6.

The cross-sectional compliance ratio is defined as $\bar{S}_{34}/\bar{S}_{33}$ where the cross-sectional compliance, $[\bar{S}]$, is the inverse of the cross-sectional stiffness, $[D]$. Cross-sectional compliance ratios for the 4 laminate styles are given in Table 7 and plotted in Figure 7. For the laminate the compliance ratio S_{16}/S_{11} (or coupling coefficient) is given in Table 4 and plotted in Figure 7. For reference a $\pm 5\%$ variation of the laminate compliance ratio is also shown. The results for all cross-sections are consistently in very good agreement with the laminate results.

To further explain and understand the differences between laminate and cross-sectional results, compliance and stiffness coupling terms are tabulated in Table 8, where the laminate compliance terms are the same as the results given by equations 2 and 3. The various coupling ratios can be described as follows: (1)S_{16}/S_{11} is the ratio of laminate shear strain to laminate axial strain due to an axial stress, (2)A_{16}/A_{11} is the ratio of laminate shear stress to laminate axial stress due to an axial strain, (3)$\bar{S}_{34}/\bar{S}_{33}$ is the ratio of cross-sectional shear strain to cross-sectional bending strain due to a bending moment, (4)D_{34}/D_{33} is the ratio of cross-sectional bending moment to cross-sectional torsional moment due to a bending strain. The compliance ratios $\bar{S}_{34}/\bar{S}_{33}$ and S_{16}/S_{11} are both consistent since an applied bending moment at the cross-section level is equivalent to a laminate level axial stress in the flanges. On the other hand, the stiffness ratios D_{34}/D_{33} and A_{16}/A_{11} are measures of the moments and stresses due to a cross-sectional bending strain and a laminate axial strain. In general, these two strain fields are equivalent only when the cross-section and the laminate are both restrained such that θ and γ_{xy} are zero. Furthermore, since the cross-section finite element model is capable of local cross-sectional distortions, laminate level shear strains (in the cross-sectional model) can occur even when θ is zero. The conclusion is that the stress fields at the laminate and cross-sectional levels are equivalent, but the strain fields are not. Further study is required to determine whether this same conclusion always applies to bend-twist coupled blade designs.

Table 5. Cross-sectional stiffness ratio.

				NACA 0012		
Laminate	Angle	Box	Circular	Single-Cell	Two-Cell	Three-Cell
Stiffness coupling ratio						
2	10	0.0722	0.0824	0.0395	0.0395	0.0526
3	15	0.0943	0.1085	0.0465	0.0467	0.0672
4	20	0.1041	0.1208	0.0464	0.0467	0.0720
5	25	0.1027	0.1201	0.0420	0.0424	0.0686
Normalized stiffness coupling ratio						
2	10	0.693	0.682	0.849	0.846	0.730
3	15	0.906	0.898	1.000	1.000	0.933
4	20	1.000	1.000	0.997	1.000	1.000
5	25	0.986	0.995	0.903	0.908	0.953

Table 6. Laminate Stiffness ratio.

Laminate	Angle	A_{16}/A_{11}	A^*_{16}/A^*_{11}
Actual value			
2	10	0.100	0.099
3	15	0.147	0.144
4	20	0.190	0.179
5	25	0.227	0.200
Normalized value			
2	10	0.439	0.496
3	15	0.646	0.718
4	20	0.836	0.896
5	25	1.000	1.000

Table 7. Cross-sectional compliance ratio.

				NACA 0012		
Laminate	Angle	Box	Circular	Single-Cell	Two-Cell	Three-Cell
Compliance coupling ratio						
2	10	0.626	0.585	0.190	0.195	0.255
3	15	0.682	0.638	0.207	0.213	0.294
4	20	0.638	0.597	0.194	0.200	0.288
5	25	0.553	0.517	0.168	0.173	0.256
Normalized compliance coupling ratio						
2	10	0.917	0.917	0.917	0.914	0.865
3	15	1.000	1.000	1.000	1.000	1.000
4	20	0.936	0.936	0.936	0.938	0.978
5	25	0.811	0.811	0.811	0.815	0.870

Table 8. Summary of Compliance and Stiffness Ratios.

	Compliance	Stiffness
Laminate	$\begin{Bmatrix} \epsilon_{xx} \\ \gamma_{xy} \end{Bmatrix} = \begin{bmatrix} S_{11} & S_{16} \\ S_{16} & S_{66} \end{bmatrix} \begin{Bmatrix} \bar{\sigma}_{xx} \\ \bar{\tau}_{xy} \end{Bmatrix}$ $\epsilon_{xx} = S_{11}\bar{\sigma}_{xx} \quad \gamma_{xy} = S_{16}\bar{\sigma}_{xx}$ $\gamma_{xy}/\epsilon_{xx} = S_{16}/S_{11}$	$\begin{Bmatrix} \bar{\sigma}_{xx} \\ \bar{\tau}_{xy} \end{Bmatrix} = \begin{bmatrix} A_{11} & A_{16} \\ A_{16} & A_{66} \end{bmatrix} \begin{Bmatrix} \epsilon_{xx} \\ \gamma_{xy} \end{Bmatrix}$ $\bar{\sigma}_{xx} = A_{11}\epsilon_{xx} \quad \bar{\tau}_{xy} = A_{16}\epsilon_{xx}$ $\bar{\tau}_{xy}/\bar{\sigma}_{xx} = A_{16}/A_{11}$
Cross-Section	$\begin{Bmatrix} \kappa_y \\ \theta \end{Bmatrix} = \begin{bmatrix} \bar{S}_{33} & \bar{S}_{34} \\ \bar{S}_{34} & \bar{S}_{44} \end{bmatrix} \begin{Bmatrix} M_x \\ T \end{Bmatrix}$ $\kappa_y = \bar{S}_{33}M_x \quad \theta = \bar{S}_{34}M_x$ $\theta/\kappa_y = \bar{S}_{34}/\bar{S}_{33}$	$\begin{Bmatrix} M_x \\ T \end{Bmatrix} = \begin{bmatrix} D_{33} & D_{34} \\ D_{34} & D_{44} \end{bmatrix} \begin{Bmatrix} \kappa_x \\ \theta \end{Bmatrix}$ $M_x = D_{33}\kappa_y \quad T = D_{34}\kappa_y$ $T/M_x = D_{34}/D_{33}$

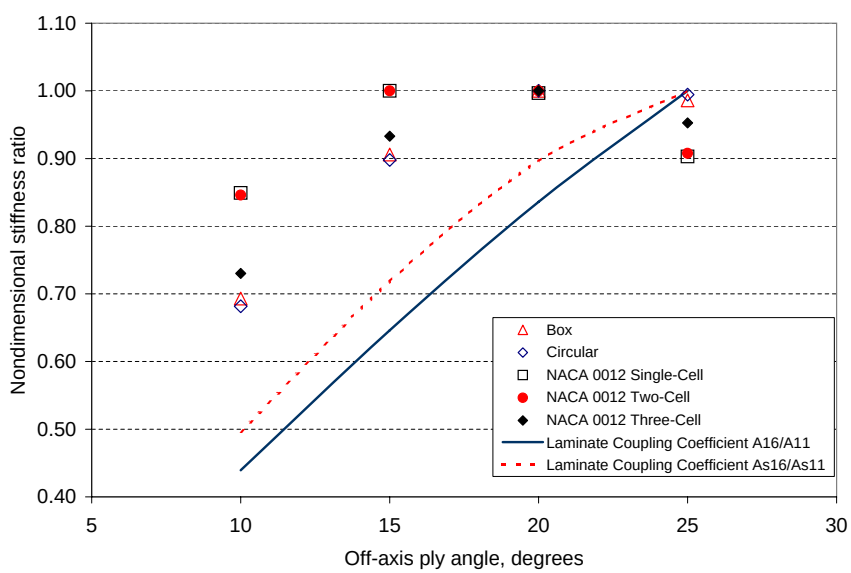

Figure 6. Comparison of cross-sectional stiffness ratio with laminate stiffness ratio.

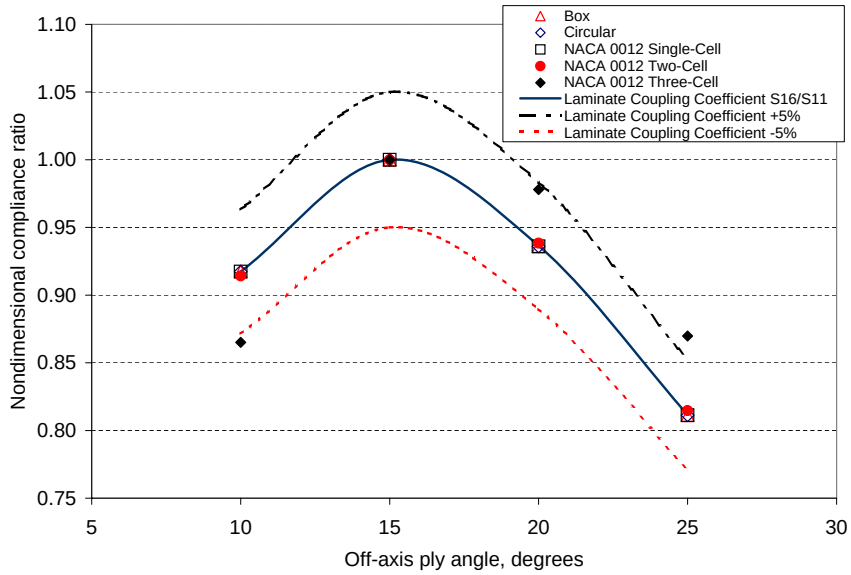

Figure 7. Comparison of cross-sectional compliance ratio with laminate compliance ratio.

IV. Conclusions and Recommendations

This paper examined the effect of coupling at the laminate level on coupling at the structural level. Four extension-shear coupled laminates are examined. The laminates are then used in structures with circular and square cross-sections followed by cross-sections representative of wind turbine blades. The properties of those cross-sections were used to describe a general elastic beam using a method from Kosmatka.

Laminate and cross-sectional coupling were compared using a normalized coupling coefficient, stiffness coupling ratio and compliance coupling ratio. Normalized coupling coefficients and stiffness coupling ratios did not compare well between the laminate and the sections. The normalized compliance ratio compared well between the laminate and the cross-sections for all cross-sections. The worst correlation of the normalized compliance ratio was observed between the laminate and the three-cell airfoil.

Acknowledgment

Development of the laminate coupling data and the tools for calculating the cross-sectional properties was supported by the U.S. Department of Energy through a subcontract from Wetzel Engineering, Inc., serving as prime contractor to US DOE via Agreement number DE-FG02-03ER86175. Dr. John B. Cadogan was the US DOE Project Officer, and Dr. Kyle K. Wetzel served as the technical monitor.

References

[1]Griffin, D., "Blade System Design Studies Volume II: Preliminary Blade Designs and Recommended Test Matrix," Sand–2004–0073, Sandia National Laboratories, 2004.

[2]TPI Composites, Inc., "Innovative Design Approaches for Large Wind Turbine Blades Final Report," Sand–2004–0074, Sandia National Laboratories, 2004.

[3]Ong, C.-H. and Tsai, S. W., "The Use of Carbon Fibers in Wind Tubine Blade Design: a SERI-8 Blade Example," Tech. Rep. SAND2000-0478, Sandia National Laboratories, 2001.

[4]Joosse, P. A., van Delft, D. R. V., Kensche, C., Jacobsen, T. K., and van den Berg, R. M., "Economic use of carbon fibres in large wind turbine blades?" *2000 ASME Wind Energy Symposium*, AIAA/ASME, Washington, DC, 2000.

[5]Lobitz, D. W., Veers, P. S., Eisler, G., Laino, D. J., Migliore, P. G., and Bir, G., "The Use of Twisted-Coupled Blades to Enhance the Performance of Horizontal Axis Wind Turbines," Tech. Rep. SAND2001-1303, Sandia National Laboratories, 2001.

[6]Locke, J. E. and Contreras, I., "The Implementation of Braided Composite Materials in the Design of a Bend-Twis Coupled Blade," Tech. Rep. SAND2002-2425, Sandia National Laboratories, 2002.

[7]de Goeij, W. C., van Tooren, M. J. L., and Beukers, A., "Implementation of Bending-Torsion Coupling in the Design of a Wind-Turbine Rotor-Blade," *Appied Energy*, , No. 63, 1999, pp. 191–207.

[8]Locke, J. E. and Valencia, U., "Design Studies for Twisted-Coupled Wind Turbine Blades," Tech. Rep. SAND2002-0522, Sandia National Laboratories, 2004.

[9]Griffin, D. A., "Evaluation of Design Concepts For Adaptive Wind Turbine Blades," Tech. Rep. SAND2002-2424, Sandia National Laboratories, 2002.

[10]Lobitz, D. W. and Veers, P. S., "Aeroelastic Behavior of Twist-Coupled HAWT Blades," *1999 ASME Wind Energy Symposium*, AIAA/ASME, Washington, DC, 1999.

[11]Lobitz, D. W. and Laino, D. J., "Load Mitigation with Twist-Coupled HAWT Blades," *1998 ASME Wind Energy Symposium*, AIAA/ASME, Washington, DC, 1998.

[12]Kosmatka, J. B., "On the Behavior of Pretwisted Beams With Irregular Cross-Sections," *Journal of Applied Mechanics*, Vol. 59, 1992, pp. 146–152.

[13]Jones, R. M., *Mechanics of Composite Materials*, Hemisphere Publishing Corporation, 1st ed., 1975.

[14]Reddy, J. N., *An Introduction to the Finite Element Method, Second Edition*, McGraw-Hill, 2nd ed., 1993.

A. Cross-Sectional Modeling Details

The three-dimensional strain components can be determined by differentiating equations 4, the result is

$$\begin{aligned} \epsilon_{xx} &= u_{,x} = U_{,x}, & \gamma_{xy} &= u_{,y} + v_{,x} = U_{,y} + V_{,x} \\ \epsilon_{yy} &= v_{,y} = V_{,y}, & \gamma_{yz} &= v_{,z} + w_{,y} = x\theta + W_{,y} \\ \epsilon_{zz} &= w_{,z} = e - x\kappa_x + y\kappa_y, & \gamma_{xz} &= u_{,z} + w_{,x} = -y\theta + W_{,x} \end{aligned} \tag{8}$$

Three-dimensional stresses (σ_{xx}, σ_{yy}, σ_{zz}, τ_{yz}, τ_{xz}, τ_{xy}) can be determined using Hooke's law

$$\{\sigma\} = [C]\{\epsilon\} \tag{9}$$

where

$$\begin{aligned} \{\sigma\}^T &= \{\sigma_{xx} \quad \sigma_{yy} \quad \sigma_{zz} \quad \tau_{yz} \quad \tau_{xz} \quad \tau_{xy}\} \\ \{\epsilon\}^T &= \{\epsilon_{xx} \quad \epsilon_{yy} \quad \epsilon_{zz} \quad \gamma_{yz} \quad \gamma_{xz} \quad \gamma_{xy}\} \end{aligned}$$

Expressions for the functions U, V, and W can be determined using the principle of virtual work:

$$\delta\Pi = \int_V \{\delta\epsilon\}^T\{\sigma\}dV = \int_V \{\delta\epsilon\}^T[C]\{\delta\epsilon\}dV = 0 \tag{10}$$

Since all of the strain terms are either constant or depend only on x and y, the volume integral in equation 10 can be reduced to an area integral over the cross-section. Furthermore, the functions U, V, and W can be approximated using two-dimensional finite element shape functions. The resulting element displacements are of the form

$$U = \{N(x,y)\}^T\{d_U\} \quad V = \{N(x,y)\}^T\{d_V\} \quad W = \{N(x,y)\}^T\{d_W\} \tag{11}$$

where $\{d_U\}$, $\{d_V\}$ and $\{d_W\}$ are nodal displacements. Substitution of equations 11 into equations 8 produces element strains that depend on the constants e, κ_x, y and θ as well as the nodal displacements:

$$\{\epsilon\} = [B]\{d\} + [f]\{h\} \tag{12}$$

where

$$[B] = \begin{bmatrix} \{N\}_{,x}^T & 0 & 0 \\ 0 & \{N\}_{,y}^T & 0 \\ 0 & 0 & 0 \\ 0 & 0 & \{N\}_{,y}^T \\ 0 & 0 & \{N\}_{,x}^T \\ \{N\}_{,y}^T & \{N\}_{,x}^T & 0 \end{bmatrix} \qquad \{d\} = \begin{pmatrix} d_U \\ d_V \\ d_W \end{pmatrix}$$

$$[f] = \begin{bmatrix} 0 & 0 & 0 & 0 \\ 0 & 0 & 0 & 0 \\ 1 & -x & y & 0 \\ 0 & 0 & 0 & x \\ 0 & 0 & 0 & -y \\ 0 & 0 & 0 & 0 \end{bmatrix} \qquad \{h\} = \begin{pmatrix} e \\ \kappa_x \\ \kappa_y \\ \theta \end{pmatrix}$$

and $[B]$ is the standard finite element matrix that relates the strains to the nodal displacements. Using equation 12 and taking the variation with respect to the functions U, V, and W produces virtual strains

$$\{\delta\epsilon\} = [B]\{\delta d\} \tag{13}$$

Substitution of equations 12 and 13 into equation 10 yields the following system of linear algebraic equations to solve for the nodal displacements $[\Delta]$:

$$[K][\Delta] = [R] \tag{14}$$

where

$$[K] = \sum_{i=1}^{\substack{\text{number of}\\ \text{elements}}} [K_i] \qquad [K_i] = \int_A [B]^T[C][B]dA$$

$$[R] = \sum_{i=1}^{\substack{\text{number of}\\ \text{elements}}} [R_i] \qquad [R_i] = -\int_A [B]^T[C][f]dA$$

$$[\Delta] = \begin{bmatrix} \{D_1\} & \{D_2\} & \{D_3\} & \{D_4\} \end{bmatrix}$$

and $[K_i]$ and $[R_i]$ are element matrices, and the displacement vectors $\{D_1\}$ through $\{D_4\}$ are the nodal displacements corresponding to "unit" values of the strain measures. That is, for displacement vector $\{D_1\}$, the strain measure vector is $\{h_1\}$ where $\{h_1\}^T = \{1 \quad 0 \quad 0 \quad 0\}$, for displacement vector $\{D_2\}$ it is $\{h_2\}^T = \{0 \quad 1 \quad 0 \quad 0\}$, etc. Thus, the element displacement vector $\{d\}$ can be written as

$$\{d\} = [\Delta_i]\{h\} \tag{15}$$

where $[\Delta_i]$ is the element $[\Delta]$ matrix. Substitution of equation 15 into equation 12 yields the following strain vector for each element

$$\{\epsilon\} = \big([B][\Delta_i] + [f]\big)\{h\} \tag{16}$$

With the strains determined, element stresses can be determined using equation 9:

$$\{\sigma\} = [C]\{\epsilon\} = [C]\big([B][\Delta_i] + [f]\big)\{h\} \tag{17}$$

The desired cross-sectional stiffness matrix can be obtained by integrating the stresses over the cross-section. This produces stress resultants (Figure 2) that are defined as

$$P = \int_A \sigma_{zz} dA \qquad M_x = \int_A y\sigma_{zz} dA$$

$$T = \int_A (x\tau_{yz} - y\tau_{xz})dA \qquad M_y = -\int_A x\sigma_{zz} dA \tag{18}$$

For each element, these stress resultants can be written in matrix form as

$$\{F_i\} = \int_A [f]^T \{\sigma\} dA = \left(\int_A [f]^T [C][B] dA [\Delta_i] + \int_A [f]^T [C][f] dA \right) \{h\} \tag{19}$$

where

$$\{F_i\}^T = \{P \quad M_y \quad M_x \quad T\}_i$$

Summing over all of the elements produces the result

$$\{F_E\} = [D]\{h\} \tag{20}$$

where

$$[D] = [D_1] - [R]^T [\delta] \tag{21}$$

$$\begin{aligned} [D_1] &= \sum_{i=1}^{\substack{\text{number of}\\ \text{elements}}} \int_A [f]^T [C][f] dA \\ -[R]^T [\delta] &= \sum_{i=1}^{\substack{\text{number of}\\ \text{elements}}} \int_A [f]^T [C][B] dA [\delta_i] \\ \{F_E\}^T &= \{F\}^T = \{P \quad M_y \quad M_x \quad T\} \end{aligned} \tag{22}$$

$[D]$ is the desired cross-sectional stiffness matrix, and the subscript "E" denotes forces due to elastic deformation

A.A. Element Coordinate System

All stress-strain relations are based on orthotropic material properties for each layer of material. These properties are specified in the material 1, 2, 3 coordinate system shown in Figure 8. The transformation from material 1, 2, 3 coordinates to global x, y, z coordinates consists of two steps. First, the transformation is determined between material 1, 2, 3 coordinates and element $\bar{x}$, $\bar{y}$, $\bar{z}$ coordinates. The material 1, 2 axes are obtained by rotating the element $\bar{x}$, $\bar{y}$ axes through an angle θ about the $\bar{z}$ axis as shown in Figure 8. Note that the material 3 axis coincides with the element $\bar{z}$ axis. The second transformation is between element $\bar{x}$, $\bar{y}$, $\bar{z}$ coordinates and global x, y, z coordinates. The element $\bar{y}$, $\bar{z}$ axes are obtained by rotating the global x, y axes through an angle α about the z axis as shown in Figure 9. Note that the element $\bar{x}$ axis coincides with the global z axis. In general, the angle α will vary within an element and must be determined by evaluating the Jacobian matrix.

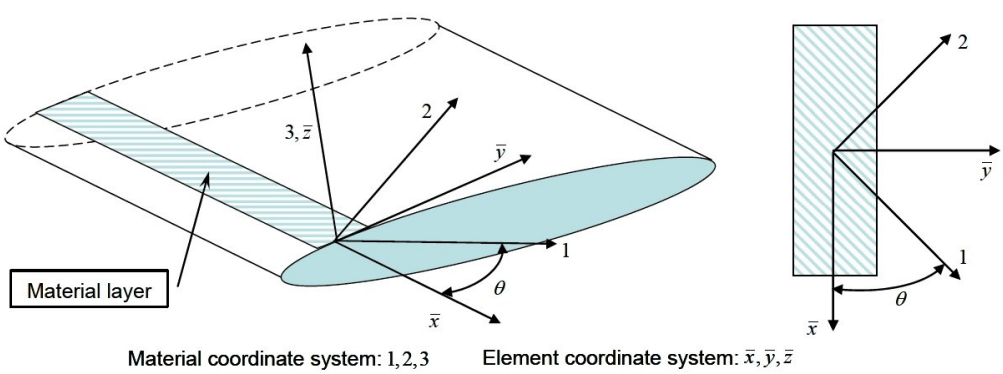

Figure 8. Beam cross-section material and element coordinate systems.

A.B. Element Shape Functions

Rectangular Lagrange quadratic elements,[14] Figure 10, were chosen for the current cross-sectional modeling approach. These elements are used to interpolate the element displacements and the cross-sectional geometry. The element shape functions are given in equation 23.

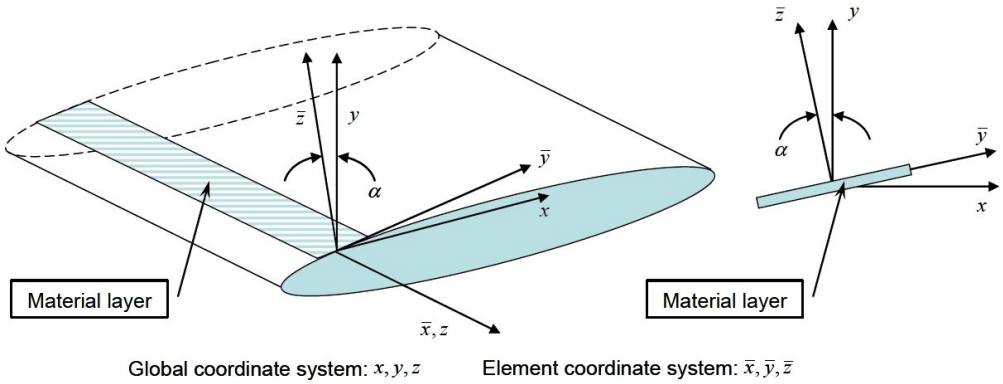

Figure 9. Beam cross-section element and global coordinate systems.

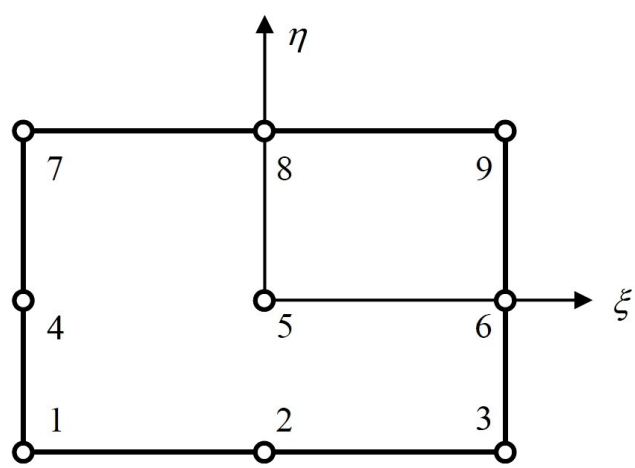

Figure 10. Nine node Lagrange quadratic element.

$$
\begin{aligned}
N_1 &= \tfrac{1}{4}(\xi^2-\xi)(\eta^2-\eta) & N_2 &= \tfrac{1}{2}(1-\xi^2)(\eta^2-\eta) & N_3 &= \tfrac{1}{4}(\xi^2+\xi)(\eta^2-\eta) \\
N_4 &= \tfrac{1}{2}(\xi^2-\xi)(1-\eta^2) & N_5 &= (1-\xi^2)(1-\eta^2) & N_6 &= \tfrac{1}{2}(\xi^2+\xi)(1-\eta^2) \\
N_7 &= \tfrac{1}{4}(\xi^2-\xi)(\eta^2+\eta) & N_8 &= \tfrac{1}{2}(1-\xi^2)(\eta^2+\eta) & N_9 &= \tfrac{1}{4}(\xi^2+\xi)(\eta^2+\eta)
\end{aligned} \tag{23}
$$

The cross-section is modeled based on defining the element ξ coordinate in the positive s direction as shown in Figure 11.

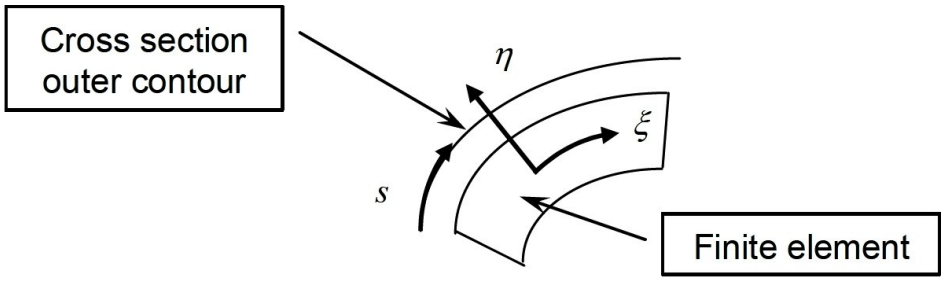

Figure 11. Positive s direction for element coordinate.